Zircon U–Pb dating of the Montredon-Labessonnié orthogneiss by LA–ICP–MS: new evidence for late Ediacaran crustal melting in the French Massif Central

Datation U–Pb sur zircon de l'orthogneiss de Montredon-Labessonnié par LA–ICP–MS : identification d'un nouveau marqueur de l'épisode de fusion crustale fini-Édiacarien dans le Massif Central français

Simon COUZINIÉ[1]*
Oscar LAURENT[2 3]

Géologie de la France, n° 2, 2021, p. 24-31, 3 fig., 2 tabl.

Keywords: Zircon U–Pb geochronology, Crustal melting, French Massif Central, Montagne Noire, Cadomian orogeny, Variscan orogeny.

Mots-clés : Géochronologie U – Pb zircon, Fusion crustale, Massif Central français, Montagne Noire, Orogenèse Cadomienne, Orogenèse Varisque.

Abstract

Unravelling the pre-Variscan evolution of the French Massif Central (FMC) demands an accurate assessment of the origin and emplacement age of the numerous meta-igneous rocks present throughout the metamorphic nappe pile. Among those, the Montredon–Labessonnié orthogneiss is a metagranite body exposed in the low-grade domain of the northern Montagne Noire. New results of LA–ICP–MS zircon U–Pb dating demonstrate that its granitic protolith was emplaced at 544.0±6.2 Ma. Whole-rock major element geochemistry, zircon crystal morphologies and the inherited zircon date distribution collectively indicate that the protolith formed by melting of Ediacaran sedimentary rocks. This orthogneiss thus represents a newly identified marker of the latest Ediacaran magmatic event well-recorded in the FMC.

Résumé

Déchiffrer l'histoire pré-Varisque du Massif Central français requiert une bonne connaissance de l'origine et de l'âge de mise en place des protolithes des roches métamorphiques ortho-dérivées. L'orthogneiss de Montredon–Labessonnié est un métagranite affleurant au niveau des nappes de faible degré métamorphique qui constituent le versant nord de la Montagne Noire. La datation U–Pb de zircons par LA–ICP–MS permet d'attribuer au protolithe un âge de mise en place de 544,0±6,2 Ma. La composition chimique en éléments majeurs de l'orthogneiss, la morphologie des grains de zircon et la gamme d'âge des zircons hérités indiquent que le protolithe granitique était issu de la fusion de roches sédimentaires édiacariennes. Cet orthogneiss constitue un nouveau marqueur d'un important épisode magmatique de la fin de l'Édiacarien représenté par plusieurs ensembles de roches ortho-dérivées du Massif Central.

1. Introduction

Over the past 20 years, the advent of in situ zircon U–Pb dating techniques (SIMS and LA–ICP–MS) has greatly improved our understanding of the pre-Variscan evolution of the continental crust exposed in the French Massif Central (FMC), notably in the Limousin (Melleton *et al.*, 2010 and references therein), Velay (Chelle-Michou *et al.*, 2017; Couzinié *et al.*, 2017, 2019), Rouergue (Lotout e*t al.*, 2017) and Montagne Noire (Cocherie *et al.*, 2005; Faure *et al.*, 2010; Padel *et al.*, 2017; Pitra *et al.*, 2012; Roger *et al.*, 2004) areas (Fig. 1). First, the high spatial resolution of these geochronological methods crucially clarified the crystallization age of the abundant meta-igneous bodies as they allowed to selectively date magmatic rims and inherited zircon cores. The occurrence of such core–rim relationships hindered earlier attempts to obtain meaningful concordant U–Pb dates based on multi-grain dissolution followed by TIMS analyses. Second, the high throughput of the LA–ICP–MS technique offered the possibility to rapidly derive representative detrital zircon date distributions and thus provided novel perspectives to unravel the depositional ages and origin of the thick and azoic (meta)sedimentary successions typically observed throughout the FMC.

Recent geochronological results along with bio–/lithostratigraphic data acquired on the weakly metamorphic sediments from the Montagne Noire (Alvaro *et al*., 2014; Devaere *et al*., 2013; Guérangé-Lozes and Burg, 1990) collectively indicate that the exposed pre-Variscan crust of the FMC was built up by Ediacaran (<590 Ma) to Silurian sedimentary rocks intruded by (mostly) granitic and basaltic magmas during apparently

[1] Université de Lorraine, CNRS, CRPG, F-54000 Nancy, France
[2] ETH Zürich, Department Erdwissenschaften, Institute for Geochemistry and Petrology, Clausiusstrasse 25, CH-8092 Zürich, Switzerland
[3] CNRS, Observatoire Midi-Pyrénées, Géosciences Environnement Toulouse, 14 avenue E. Belin, F-31400 Toulouse, France

*Corresponding author: simon.couzinie@univ-lorraine.fr

Manuscrit reçu le 12 mars 2021, accepté le 16 juin 2021

two key time periods: the late Ediacaran–earliest Cambrian (550–530 Ma), the latest Cambrian (Furongian) to Ordovician (500–450 Ma). Magmatic products were both volcanic (lavas or pyroclastic flows, volcaniclastic sediments) and plutonic, forming intrusive bodies within the sedimentary rocks (Laumonier *et al.*, 2004).

Among the pre-Variscan igneous rocks, the Montredon–Labessonnié orthogneiss in the northern Montagne Noire (Fig. 1) stands as a notable chronological exception. Indeed, the currently retained zircon U–Pb emplacement age of its granitic protolith is 717+83/-55 Ma (Guérangé-Lozes, 1987), making it the oldest rock dated so far in the FMC. Importantly, this Cryogenian age was obtained via multi-grain dissolution procedures and corresponds to an upper intercept from a set of discordant analyses. In light with the common presence of inherited zircon cores in similar rocks from the FMC (Couzinié *et al.*, 2017), it may not represent the actual crystallization age of the parental magma. In this short contribution, we revaluate the age of the Montredon–Labessonnié orthogneiss protolith and address its petrogenesis based on new LA–ICP–MS U–Pb zircon analyses and available geochemical data.

2. Geological setting and sample description

The northern part of the Montagne Noire (Fig. 1) exposes a set of low-grade (chlorite zone) nappes (the Albigeois and Mont-de-Lacaune units) separated by top-to-the S thrusts and structurally overlying a medium- to high-grade domain referred to as the “axial zone” (Demange, 1994; Gèze, 1949). The latter encompasses (meta)sedimentary sequences (Saint–Pons and La Salvetat formations) deposited in the Ediacaran (Lescuyer and Cocherie, 1992) and two granitic orthogneisses: the voluminous Somail–Nore suite of Ordovician (470–455 Ma) age (Cocherie *et al.*, 2005; Roger *et al.*, 2004) and the Plaisance–Cammazes orthogneiss, dated at 550±5 Ma (Guérangé-Lozes *et al.*, 2013). The so-called Albigeois unit (Guérangé-Lozes and Burg, 1990; Alvaro *et al.*, 2014) is composed of: (i) Cambrian to Lower Ordovician sedimentary rocks; (ii) felsic (sub)volcanic rocks of late Cambrian (Furongian) age; (iii) basaltic lava flows interbedded within late Cambrian and (largely) Lower Ordovician series (Marini, 1987). The Monts-de-Lacaune unit (Fig. 1) comprises several Ediacaran to Lower Ordovician sedimentary successions plus a Silurian formation. Interlayered volcanics include the 200m-thick rhyolitic tuffs of the Rivernous Formation, dated at c. 540 Ma (Padel *et al.*, 2017) and the 300m-thick basaltic Ensèges Volcanic Complex, of presumably Lower Cambrian age (Guérangé-Lozes and Burg, 1990; Alvaro *et al.*, 2014). Two orthogneiss massifs crop out in the Monts-de-Lacaune (Fig. 1): (i) the “Mendic granite” to the East, emplaced within the Ediacaran Grandmont formation at 507±10 Ma (whole-rock Rb–Sr, recalculated by Demange, 1982, based on data from Hamet and Allègre, 1973); (ii) the Montredon–Labessonnié orthogneiss to the West forms the core of a NE–SW antiform and is structurally overlain by biotite-bearing micaschists, dolostones and (meta)black shales with phosphatic nodules, the latter two being correlated to Lower Cambrian formations (Béziat *et al.*, 1980). Orthogneisses and micaschists are the host of a c. 315 Ma-old (Harlaux *et al.*, 2018) tungsten mineralization which would be related to the intrusion of an unexposed granite body.

A sample of the equigranular facies (Barras, 1979) of the Montredon–Labessonnié orthogneiss was collected from the core of the massif (GPS coordinates: 43.73238, 2.32221). The sample shows an augen mylonitic texture defined by 0.5–1 cm-large polymineralic K-feldspar and plagioclase aggregates (both studded with fine muscovite inclusions) separated from fine-grained (c. 500µm) mosaic quartz ribbons by muscovite and chlorite (after biotite) flakes underlining the foliation (Fig. 2a,b). Ovoid, mm-sized bluish quartz crystals are scattered throughout the rock and most likely represent relict igneous grains (Seifert *et al.*, 2011). Evidence for interaction with hydrothermal to meteoric fluids include red clouding of K-feldspar, sporadic occurrence of tourmaline and recrystallization of biotite to chlorite.

The whole-rock major element composition of the dated sample was obtained from the ALS Global company (measured by ICP–AES, Table 1, further details on the analytical routines can be found at http://www.alsglobal.com/). The dated sample is highly silicic (SiO_2=76.0 wt.%, Fig. 2c,d,e), classifies as a potassic (K/(Na+K)=0.53) peraluminous leucogranite I following Debon and Le Fort (1988) and plots in the field of calc-alkaline suites in the sense of Frost *et al.* (2001). A comparison with analyses of fresh to poorly altered orthogneiss samples reported by Guion (1984) highlights that the dated rock is fairly representative of the Montredon–Labessonnié orthogneisses (Fig. 2c,d,e).

3. Zircon U – Pb dating

Zircon grains were separated using standard techniques (jaw crusher, panning, heavy liquids) and c. 80 selected grains were cast in epoxy resin and polished down to a near-equatorial grain section. Cathodoluminescence imaging was performed at the Laboratoire Magmas et Volcans (Clermont-Ferrand, France) using a Jeol JSM-5910. ZirconU–Pb isotopic analyses were carried out at ETH Zürich, Switzerland by laser ablation–inductively coupled plasma–sector field–mass spectrometry using a RESOlution (ASI, Australia) 193 nm ArF excimer laser system attached to an Element XR (Thermo Scientific, Germany) mass spectrometer. The analytical procedure was identical to that described in Couzinié *et al.* (2019). Age calculations and data plotting were performed using IsoplotR (Vermeesch, 2018). Systematic uncertainties were propagated to the weighted average dates (Fig. 3c) following the scheme of Horstwood *et al.* (2016). Those include the uncertainties on: (i) the decay constants for ^{238}U and ^{235}U, set at 0.107% and 0.136% for ^{238}U and ^{235}U, respectively (Jaffey *et al.*, 1971); (ii) the isotope ratios of the primary standard (GJ–1), set at 0.5%; (iii) the overall reproducibility of the method, estimated based on the long-term excess scatter of secondary zircon reference materials, i.e. 1% relative in the ETH lab. Error propagation involved the quadratic addition of the “internal” error calculated by IsoplotR (which already includes uncertainties on the decay constants) and the other systematic errors listed above. The accuracy of the corrections was checked by analysing secondary zircon reference materials 91500 (Wiedenbeck *et al.*, 1995), Temora (Black *et al.*, 2003) and Plešovice (Sláma *et al.*, 2008), and all yielded accurate dates within the above considered reproducibility of the method (Table 2).

Zircon grains are euhedral and range in size between 80 and 250 µm (and in few cases up to 500 µm) with aspect ratios of 2 to 3. Examination of external morphologies and CL growth zoning patterns (following the approach of Vavra, 1994) consistently indicate that the {110} prism faces are more developed than the {100} forms (Fig. 3a). Besides, {121} pyramids are conspicuous. Most grains display well-developed, concentric oscillatory zoning and core–rim relationships are very common. Local truncations in the growth patterns (e.g. top left zircon in Fig. 3a) evidence intermittent stages of crystal corrosion, consistent with local and transient undersaturation of the melt phase from which the grains crystallized. Forty-four analyses were performed on oscillatory-zoned zircon grains and rims, 40 of which yielded concordant $^{206}Pb/^{238}U$ dates ranging between 568±6 (#20) and 529±4 Ma (#45), the remaining analyses being discordant (Fig. 3b). Among the 21 analysed cores, 14 showed concordant $^{206}Pb/^{238}U$ dates between 1490±19 (#33) and 579±6 Ma (#29). The other cores yielded discordant results, 3 of them showing Neoarchean to Paleoproterozoic $^{207}Pb/^{206}Pb$ dates of 2758±19 (#66), 2395±9 (#49) and 2334±14 Ma (#28). The calculated density plot shows a minor peak centred at c. 564 Ma and a major one at c. 544 Ma, the shape of which is slightly asymmetric and skewed towards younger ages (Fig. 3c). For the main peak, a weighted average $^{206}Pb/^{238}U$ date of 544.0±6.2 Ma (MSWD=1.2) can be calculated out of 27 analyses centred on the symmetric part of the distribution. For the minor, older one, a weighted average $^{206}Pb/^{238}U$ date of 563.9±6.6 Ma (MSWD=1.3) was obtained based on 7 analyses.

4. Discussion

Most oscillatory-zoned magmatic grain domains yielded U–Pb dates clustered around c. 544 Ma. Therefore, we interpret the average date of 544.0±6.2 Ma as the crystallization age of the Montredon–Labessonnié orthogneiss protolith. The 6 grains showing younger concordant dates spanning down to 529±4 Ma (Fig. 3b,c) would correspond to magmatic grains from the main population having experienced variable still limited Pb loss, as suggested by the negatively skewed date distribution (Spencer *et al.*, 2016). This view is further supported by the local occurrence of convolute zoning in some of these grains (e.g. bottom right zircon on Fig. 3a) which provides textural evidence for post-crystallization elemental diffusion (Corfu *et al.*, 2003). The c. 564 Ma oscillatory-zoned grains seem devoid of younger overgrowths but are often corroded (bottom left zircon on Fig. 3a) which points to either mechanical abrasion (the grains are detrital) or/and partial dissolution in a zircon-undersaturated granitic melt. Therefore, they most likely represent inherited grains from the magma source or xenocrysts incorporated during magma ascent and emplacement. This interpretation can also be retained for the Paleoproterozoic to Neoproterozoic zircon cores overgrown by c. 544 Ma-old rims.

Several pieces of evidence suggest that the protolith of the Montredon–Labessonnié orthogneiss formed by melting of pre-existing crustal lithologies. First, the orthogneiss samples define a peraluminous calc-alkaline to alkali-calcic association (Fig. 2c,d,e) as typically observed in crust-derived granitic suites (Bonin *et al.*, 2020). As a matter of fact, their compositions largely overlap with that of the Velay orthogneisses (Fig. 2c,d,e), the protoliths of which demonstrably are crust-derived granites (Couzinié *et al.*, 2017). Second, the predominance of {110} and {121} crystal forms in the magmatic crystals and the marked zircon inheritance are features commonly observed in crust-derived magmas (Pupin, 1980; Vavra, 1994). Third, the inherited zircon grains and cores in the Montredon–Labessonnié orthogneiss yielded Neoarchean–Paleoproterozoic and Neoproterozoic dates (down to c. 564 Ma), as observed in their Velay counterparts (Couzinié *et al.*, 2021, 2017). Detrital zircon grains with identical ages are widespread in the Ediacaran (meta)sedimentary sequences of the FMC and attest to the recycling of an old Gondwana basement (African cratons) and Cadomian (or Panafrican) magmatic arcs (Chelle-Michou *et al.*, 2017; Couzinié *et al.*, 2019; Melleton *et al.*, 2010). Based on their inherited zircon date distribution, the Montredon–Labessonnié (meta)granite most likely formed by melting of Ediacaran sedimentary rocks.

The zircon crystallization age of 544±6.2 Ma obtained for the Montredon–Labessonnié orthogneiss protolith is identical within error to those of several meta-igneous rocks from the Montagne Noire such as the Rivernous rhyolites, the Plaisance–Cammazes orthogneisses and the Sériès metadacites (Guérangé-Lozes *et al.*, 2013; Lescuyer and Cocherie, 1992; Padel *et al.*, 2017). It also matches that of the voluminous Velay Orthogneiss Formation, exposed over 1800 km^2 in the eastern FMC (Couzinié *et al.*, 2021, 2017), and of several metagranite bodies in the Limousin area (Alexandrov *et al.*, 2001; Melleton *et al.*, 2010). Additional massifs of similar yet ill-constrained ages include the Picades and Caplongue (meta)diorites in the Lot and Rouergue area, respectively (Lafon, 1984; Pin and Lancelot, 1978). Coeval igneous rocks have also been identified in adjacent segments of the northern Gondwana margin such as: (i) the northern Armorican Massif (Mancellian granites, Egal *et al.*, 1996); (ii) the Saxo-Thuringian Zone of the Bohemian Massif (Laubach & Glasbach granites, Linnemann *et al.*, 2014); (iii) the eastern Pyrenees (Canaveilles volcanics, e.g. Padel *et al.*, 2018). Given the paleo-location of the FMC by the late Ediacaran (Couzinié *et al.*, 2019) and considering the lack of coeval regional metamorphism or compressive deformation (Alvaro *et al.*, 2014), this magmatic event should be tied to a distal manifestation of the wanning Cadomian orogeny (Garfunkel, 2015; Padel *et al.*, 2018, 2017).

Acknowledgements

The help of J.-M. Hénot with the SEM was greatly appreciated. We thank M. Faure, an anonymous reviewer, and the editor D. Thiéblemont for their comments which helped to improve the manuscript.

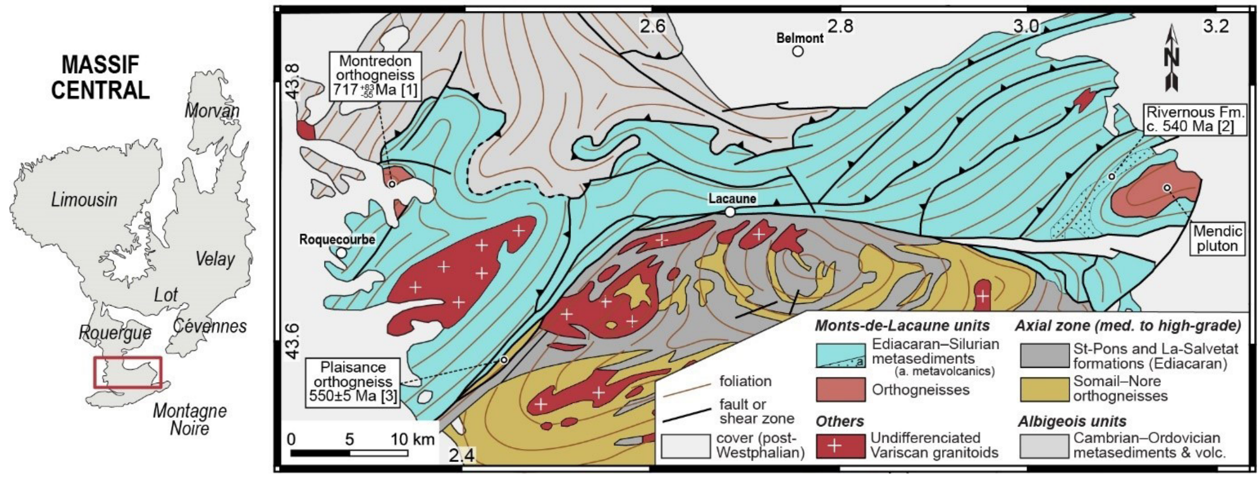

Figure 1: Location of the main geological domains of the French Massif Central and geological map of the northern Montagne Noire, depicting the main litho-tectonic associations and meta-igneous rocks, redrawn and adapted from Chantraine *et al.* (1996). References: [1] Guérangé-Lozes, 1987; [2] Padel *et al.*, 2017; [3] Guérangé-Lozes *et al.*, 2013.

Figure 1 : Localisation des principaux ensembles géologiques du Massif Central français et carte géologique simplifiée du versant nord de la Montagne Noire, figurant les principaux ensembles litho-tectoniques et les roches ortho-dérivées, redessinée et adaptée à partir de Chantraine et al. (1996). Références : [1] Guérangé-Lozes, 1987 ; [2] Padel et al., 2017 ; [3] Guérangé-Lozes et al., 2013.

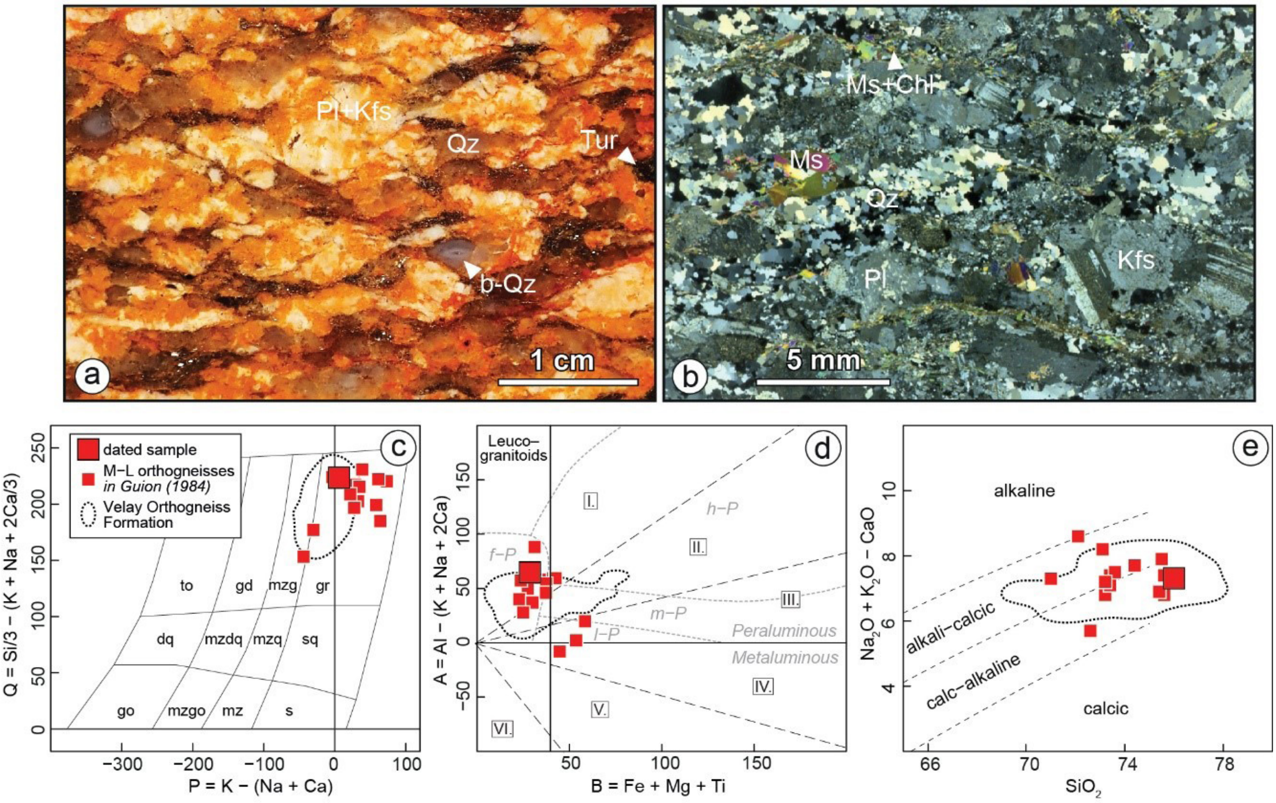

Figure 2: Petrography and whole-rock geochemistry of the Montredon–Labessonnié orthogneiss. (a) Polished rock slab and (b) thin section (crossed polars) of the dated sample highlighting the deformation of the "granitic" assemblage and the persistence of igneous bluish quartz grains (b-Qz). (c) P–Q and (d) B–A cationic classification diagrams of Debon and Le Fort (1988). (e) SiO_2 vs. MALI diagram of Frost *et al.* (2001). The subdivisions of Villaseca *et al.* (1998) are indicated in (b). Plotted using the GCDkit software (Janoušek *et al.*, 2006). The dotted black lines delineate the field containing 85% of 270 analyses of the Velay orthogneisses (Couzinié *et al.*, 2017), contoured using the kde2d function of R.

Figure 2 : Pétrographie et composition géochimique en roche totale de l'orthogneiss de Montredon–Labessonnié. (a) Section polie et (b) lame mince (vue en lumière polarisée analysée) de l'échantillon daté illustrant la déformation de l'assemblage « granitique » et la présence de quartz bleuté d'origine magmatique (b-Qz). (c,d) Diagrammes chimico-minéralogiques P–Q et B–A de Debon and Le Fort (1988). (e) Diagramme SiO_2 vs. MALI de Frost et al. (2001). Les subdivisions de Villaseca et al. (1998) sont indiquées sur le panel (b). Les diagrammes ont été tracés avec GCDkit (Janoušek et al., 2006). Les pointillés noirs délimitent le champ contenant 85 % de 270 analyses d'orthogneiss du Velay (Couzinié et al., 2017). Sa position a été calculée en utilisant la fonction kde2d de R.

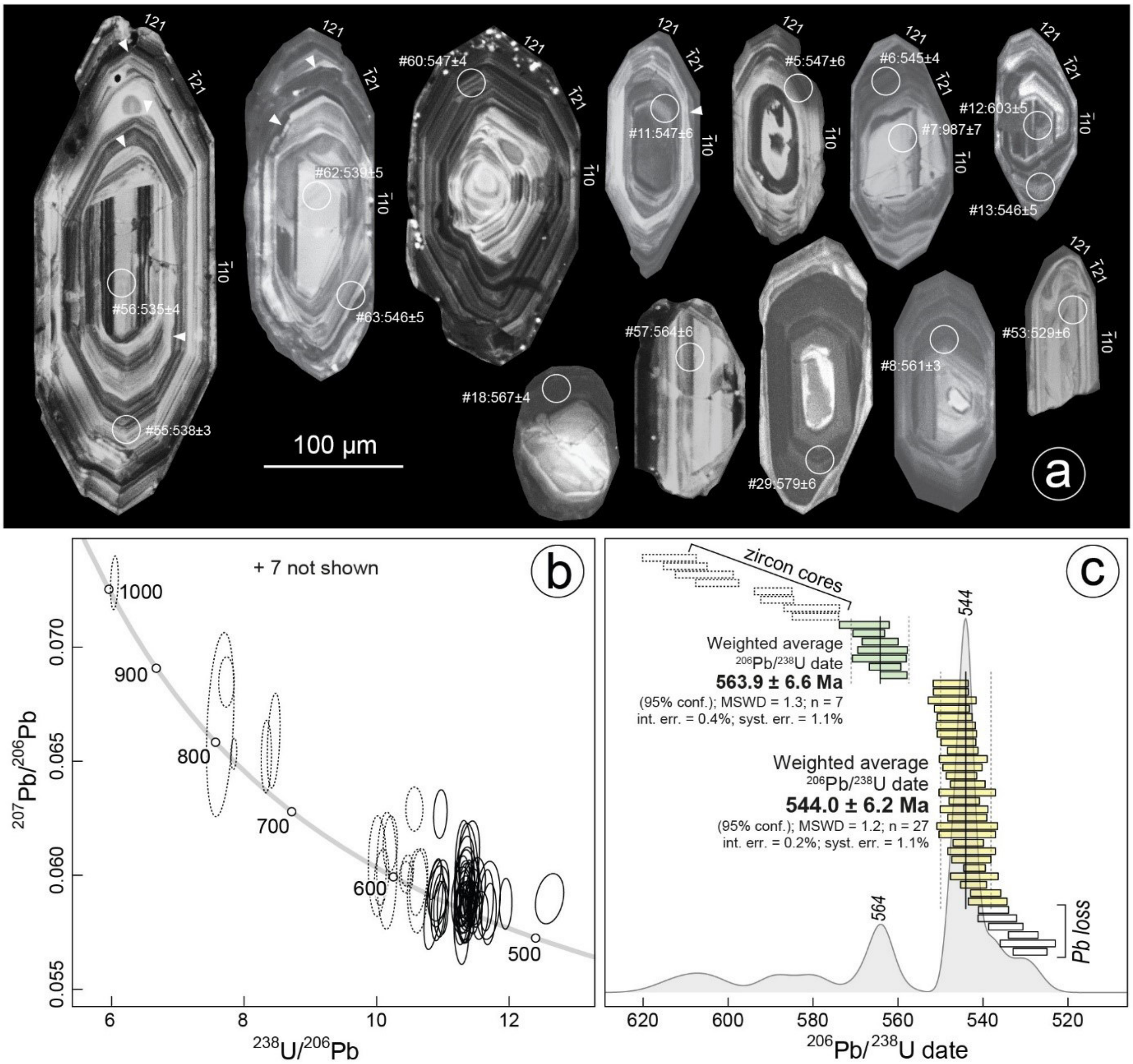

Figure 3: (a) Representative cathodoluminescence images of zircon grains from the Montredon–Labessonnié orthogneiss. The locations of laser spots are indicated along with the corresponding concordant $^{206}Pb/^{238}U$ dates, quoted with ±2σ uncertainty in Ma. The crystal faces are labelled with Miller indices following the method of Vavra (1994). All displayed grains are lying on the (110) face. White triangles highlight truncations in the growth patterns. (b) Tera-Wasserburg diagram ($^{238}U/^{206}Pb$ vs. $^{207}Pb/^{206}Pb$) with error ellipses displayed at the 95% level of confidence. Analyses were not corrected from common Pb. (c) Ranked concordant $^{206}Pb/^{238}U$ dates of Neoproterozoic to Lower Cambrian zircon grains and corresponding density plot. Dotted bars refer to zircon cores. Green and yellow analyses are those considered for the weighted average date calculations.

Figure 3 : (a) Images en cathodoluminescence de grains de zircons extraits de l'orthogneiss de Montredon–Labessonnié. Sont indiquées la localisation des points d'analyse ainsi que l'âge $^{206}Pb/^{238}U$ correspondant, en Ma. Les erreurs sont données à ±2σ. Les faces cristallines sont indexées par leurs indices de Miller en se basant sur la méthode de Vavra (1994). Tous les grains présentés reposent sur la face (110). Les triangles blancs soulignent des anomalies dans le « pattern » de croissance, reliées à des épisodes de corrosion. (b) Diagramme de Tera-Wasserburg ($^{238}U/^{206}Pb$ vs. $^{207}Pb/^{206}Pb$) où les ellipses représentent l'incertitude à 95 % de confiance. Les analyses n'ont pas été corrigées de la présence de plomb commun. (c) Représentation des âges $^{206}Pb/^{238}U$ pour les zircons néoprotérozoïques et cambriens, avec en surimposition le diagramme de densité. Les analyses en pointillés correspondent aux cœurs de zircons. Les analyses en vert et en jaune sont celles prises en compte pour le calcul de l'âge moyen.

SiO_2	Al_2O_3	Fe_2O_3	MnO	MgO	CaO	Na_2O	K_2O	TiO_2	P_2O_5	LOI
76.00	13.80	1.98	0.03	0.12	0.34	2.84	4.81	0.07	0.32	1.32

Table 1: Major element composition of the dated sample of the Montredon–Labessonnié orthogneiss, in wt.%.

Tableau 1 : Composition en éléments majeurs de l'orthogneiss de Montredon–Labessonnié daté dans le cadre de cette étude, les concentrations sont exprimées en % poids d'oxydes.

		Concentrations (ppm)				Isotopic ratios					Dates (Ma)				
Spot	Texture	U[a]	Th[a]	Pb[a]	Th/U	$^{238}U/^{206}Pb$[b]	±2s%	$^{207}Pb/^{206}Pb$[b]	±2s%	Rho[c]	$^{207}Pb/^{206}Pb$	±2σ	$^{206}Pb/^{238}U$	±2σ	Conc.[d]
#1	rim of 2	243	29	186	0.12	11.519	0.9	0.0597	1.5	0.06	590	30	537	5	d
#10	hom. zrn	1600	98	608	0.06	10.929	1.2	0.0592	1.7	0.24	579	33	564	6	c
#11	hom. zrn	567	71	480	0.12	11.299	0.8	0.0595	1.8	0.07	588	37	547	4	c
#12	core of 13	362	180	1464	0.50	10.206	0.9	0.0614	1.6	0.09	655	31	603	5	d
#13	rim of 12	699	59	420	0.08	11.305	0.9	0.0588	1.3	0.12	561	27	546	5	c
#14	hom. zrn	233	52	328	0.22	11.280	0.8	0.0578	2.4	-0.03	513	54	548	4	c
#15	hom. zrn	853	64	397	0.08	11.319	0.8	0.0586	2.2	0.03	561	42	546	4	c
#16	core of 17	408	23	149	0.06	10.616	1.2	0.0593	2.5	0.06	574	54	581	7	c
#17	rim of 16	565	64	538	0.11	10.961	0.8	0.0627	1.4	0.13	697	26	563	4	d
#18	rim	5830	165	831	0.03	10.879	0.7	0.0598	1.2	0.59	597	23	567	4	c
#19	hom. zrn	493	46	337	0.09	11.384	0.9	0.0587	1.4	0.03	557	29	543	5	c
#2	core of 1	1140	272	2070	0.24	10.570	1.0	0.0629	1.3	0.00	703	24	583	6	d
#20	hom. zrn	331	130	940	0.39	10.858	1.1	0.0587	2.7	0.53	546	59	568	6	c
#21	rim	739	49	328	0.07	11.348	0.7	0.0593	1.7	0.03	575	35	544	4	c
#22	core of 23	614	126	1121	0.21	7.734	1.2	0.0685	1.3	0.03	882	24	784	9	d
#23	rim of 22	450	59	372	0.13	10.933	0.8	0.0586	2.0	0.33	557	40	564	4	c
#24	rim of 25	739	78	465	0.11	11.947	0.6	0.0588	1.5	0.05	561	30	518	3	c
#25	core of 24	544	378	3160	0.69	8.335	0.8	0.0652	2.0	0.08	778	40	731	5	c
#26	core	458	432	3260	0.94	8.446	0.9	0.0659	2.6	0.32	799	53	721	7	d
#27	hom. zrn	251	35	211	0.14	11.386	1.1	0.0602	2.8	-0.15	615	64	543	6	c
#28	core	450	270	5770	0.60	3.668	0.7	0.1490	1.0	0.13	2334	14	1554	9	d
#29	core	1609	94	597	0.06	10.633	1.0	0.0597	2.0	0.34	590	40	579	6	c
#3	rim of 4	306	20	127	0.06	11.459	0.7	0.0585	1.6	0.05	547	31	539	3	c
#30	hom. zrn	293	51	338	0.17	11.334	0.7	0.0581	1.5	-0.02	529	31	545	4	c
#31	hom. zrn	493	59	367	0.12	11.339	0.9	0.0605	1.7	0.24	631	41	545	5	d
#32	rim of 33	332	63	396	0.19	11.364	1.3	0.0594	2.5	0.04	575	56	543	7	c
#33	core of 32	145	194	3640	1.34	3.845	1.4	0.0929	1.3	-0.04	1488	21	1490	19	c
#34	rim	10230	1680	7800	0.16	29.291	1.1	0.0876	5.7	-0.09	1340	110	216	2	d
#35	core	81	89	754	1.11	10.152	1.2	0.0602	3.5	0.03	596	74	606	7	c
#36	core	144	126	838	0.87	10.010	1.1	0.0604	3.0	0.04	611	66	614	7	c
#37	core	1874	214	1161	0.11	10.462	0.7	0.0602	0.9	0.11	612	16	588	4	c
#38	hom. zrn	979	69	462	0.07	11.369	0.7	0.0585	1.0	0.25	548	19	543	4	c
#39	hom. zrn	274	40	281	0.15	11.343	1.1	0.0585	2.1	0.03	541	45	545	6	c
#4	core of 3	89	29	234	0.33	7.639	2.2	0.0666	5.0	0.30	840	120	793	17	c
#40	hom. zrn	376	69	499	0.18	11.396	0.6	0.0592	2.0	0.01	567	43	542	3	c
#41	rim	889	81	493	0.09	11.364	1.3	0.0587	1.4	0.76	554	28	544	7	c
#42	hom. zrn	170	51	305	0.30	11.364	1.4	0.0603	2.8	0.44	615	63	544	7	c
#43	hom. zrn	325	83	537	0.26	11.364	0.9	0.0600	1.5	-0.10	608	31	544	5	d
#44	hom. zrn	841	67	384	0.08	11.400	1.1	0.0593	1.9	0.46	577	37	542	6	c
#45	hom. zrn	218	38	261	0.17	11.695	0.8	0.0583	1.9	0.19	531	39	529	4	c
#46	hom. zrn	362	61	406	0.17	11.347	1.1	0.0586	1.6	0.18	557	32	544	6	c
#47	core	1045	552	5620	0.53	7.845	0.5	0.0653	0.9	0.18	785	13	773	3	c
#48	rim of 49	1288	81	545	0.06	11.366	0.8	0.0598	1.1	-0.20	599	23	544	4	d
#49	core of 48	345	143	4080	0.42	2.435	0.7	0.1544	0.8	-0.19	2395	9	2217	13	d
#5	rim	304	31	192	0.10	11.287	1.1	0.0589	2.0	0.10	561	41	547	6	c
#50	core	2750	6990	24700	2.54	12.853	2.3	0.0928	3.8	-0.23	1472	69	483	11	d
#51	hom. zrn	800	80	375	0.10	12.610	1.4	0.0590	1.5	0.25	564	31	492	7	d
#52	core	2700	230	1750	0.09	10.445	0.8	0.0599	0.9	0.01	600	16	589	5	c
#53	hom. zrn	347	128	820	0.37	11.682	1.3	0.0589	2.4	0.14	566	47	529	6	c
#55	hom. zrn	434	31	218	0.07	11.500	0.7	0.0586	1.2	0.01	554	23	538	3	c
#56	hom. zrn	363	82	619	0.23	11.565	0.8	0.0582	1.5	0.17	540	29	535	4	c
#57	hom. zrn	231	66	407	0.29	10.945	1.1	0.0592	2.0	0.37	582	46	564	6	c
#58	rim	967	90	579	0.09	11.279	0.8	0.0586	1.2	-0.07	551	24	548	4	c
#59	core	429	618	5760	1.44	10.075	0.9	0.0599	1.7	0.23	604	34	610	5	c
#6	rim of 7	469	50	314	0.11	11.340	0.7	0.0582	1.5	0.19	546	31	545	4	c
#60	hom. zrn	334	27	226	0.08	11.285	0.8	0.0583	1.9	0.22	551	37	547	4	c
#61	hom. zrn	227	31	224	0.14	10.957	0.7	0.0585	1.7	0.09	542	36	563	4	c
#62	hom. zrn	199	19	122	0.10	11.469	0.9	0.0591	1.7	-0.02	563	35	539	5	c
#63	hom. zrn	322	38	211	0.12	11.311	0.9	0.0602	3.0	0.05	602	65	546	5	c
#64	rim of 65	181	31	223	0.17	11.658	0.7	0.0589	1.9	0.15	564	41	531	4	c
#65	core of 64	1041	880	5070	0.85	11.990	1.6	0.0789	6.7	-0.08	1130	130	516	8	d
#66	core	1106	278	9500	0.25	2.417	2.0	0.1919	0.7	-0.37	2758	7	2230	37	d
#7	core of 6	128	73	979	0.57	6.042	0.8	0.0728	1.3	0.22	1014	26	987	7	d
#8	hom. zrn?	272	46	312	0.17	10.997	0.6	0.0586	1.6	0.10	544	33	561	3	c
#9	hom. zrn	821	78	277	0.09	11.401	0.5	0.0591	1.0	0.42	571	18	542	3	c
Z_1	Plešovice	1047	122	495	0.12	18.258	1.1	0.0538	1.7	0.07	370	38	344	4	c
Z_2		1154	184	778	0.16	18.495	0.6	0.0535	1.3	0.05	351	25	339	2	c
Z_3		578	56	238	0.10	18.292	0.6	0.0543	2.4	0.03	379	50	343	2	c
Z_4		880	136	644	0.15	18.335	0.5	0.0534	1.2	0.04	344	24	342	2	c
Z_5		842	112	494	0.13	18.396	0.5	0.0532	1.2	0.10	338	24	341	2	c
Z_6		962	109	403	0.11	18.632	1.0	0.0535	2.2	0.32	347	48	337	3	c
Z_7		605	63	267	0.10	18.549	0.5	0.0535	1.2	0.07	350	24	339	2	c
Z_8		903	156	730	0.17	18.362	0.6	0.0535	1.2	0.18	354	24	342	2	c
Z_9		624	67	294	0.11	18.406	0.6	0.0537	1.8	0.25	355	37	341	2	c
Z_10		1097	169	709	0.15	18.386	0.6	0.0539	1.5	0.20	365	31	341	2	c
Z_11		1187	169	661	0.14	18.318	1.2	0.0540	2.0	0.20	368	45	343	4	c
								Concordia age: 341.2±3.9 Ma (MWSD$_{C+E}$=1.8, n=11)							
Z_1	Temora2	120	68	361	0.57	15.198	0.8	0.0559	2.9	0.14	439	62	411	3	c
Z_3		159	58	248	0.36	15.263	1.3	0.0544	3.9	0.32	395	79	409	5	c
Z_4		83	23	110	0.28	15.337	1.5	0.0553	4.2	0.11	405	90	407	6	c
Z_5		102	41	214	0.40	15.186	0.9	0.0557	2.3	0.21	437	51	412	4	c
Z_8		273	151	800	0.55	15.056	0.7	0.0552	1.7	0.02	425	37	415	3	c
Z_9		234	137	699	0.59	15.242	0.7	0.0552	2.2	-0.08	409	47	410	3	c
Z_10		202	107	608	0.53	15.177	0.7	0.0548	2.2	0.27	403	46	411	3	c
Z_2		118	40	203	0.34	15.706	0.8	0.0561	2.5	0.13	442	57	398	3	c
Z_7		97	55	284	0.57	15.676	1.1	0.0549	3.3	0.38	400	72	399	4	c
Z_6		105	60	337	0.57	16.132	1.2	0.0623	3.9	0.23	661	79	388	4	d
								Concordia age: 411.2±4.8 Ma (MWSD$_{C+E}$=1, n=7)							
Z_1	91500	50	17	212	0.34	5.602	0.9	0.0745	2.6	0.29	1044	52	1059	9	c
Z_2		53	22	298	0.41	5.643	0.7	0.0739	2.2	0.29	1028	42	1052	7	c
Z_3		50	21	300	0.41	5.599	1.5	0.0737	2.4	0.37	1031	49	1059	14	c
Z_4		77	30	383	0.38	5.653	1.4	0.0746	2.7	0.27	1076	54	1050	13	c
Z_5		82	33	356	0.40	5.695	1.6	0.0745	3.9	0.25	1068	82	1043	15	c
Z_6		65	25	325	0.39	5.695	0.9	0.0739	2.3	-0.08	1036	43	1043	9	c
Z_7		76	30	353	0.40	5.631	1.3	0.0750	3.2	-0.03	1073	61	1054	13	c
Z_8		58	22	285	0.38	5.640	0.7	0.0745	2.1	-0.06	1052	40	1052	7	c
Z_11		41	13	180	0.32	5.612	0.9	0.0774	2.5	0.21	1123	48	1057	9	d
Z_10		50	17	233	0.35	5.663	0.9	0.0752	3.3	0.22	1089	61	1048	9	c
Z_9		50	18	268	0.36	5.727	0.7	0.0768	2.1	-0.04	1106	41	1037	7	d
								Concordia age: 1052.4±12.2 Ma (MWSD$_{C+E}$=1.3, n=10)							

Table 2: Results of LA–ICP–MS U–Pb analyses of zircon grains from the Montredon–Labessonnié orthogneiss and secondary standards, obtained with a spot size of 20µm. a U, Th and Pb contents were calculated relative to GJ-1; b values corrected for background, within-run Pb/U fractionation (in case of $^{206}Pb/^{238}U$) and subsequently normalised to GJ-1 (ID-TIMS value/measured value); c rho is the $^{238}U/^{206}Pb/^{207}Pb/^{206}Pb$ error correlation coefficient; d an analysis is labelled as concordant "c" or discordant "d" based on the overlap between the error ellipse (at 95% conf.) and the Concordia curve.

Tableau 2 : Résultats des analyses U–Pb par LA–ICP–MS réalisées sur les grains de zircons de l'orthogneiss de Montredon–Labessonnié et les standards secondaires, obtenus avec une taille de spot de 20µm. a Les concentrations élémentaires en U, Th and Pb ont été calculées relativement à GJ-1; b valeurs corrigées du bruit de fond, du fractionnement Pb/U lors de l'ablation (dans le cas de $^{206}Pb/^{238}U$) et ensuite normalisées à GJ-1 (valeur ID-TIMS / valeur mesurée) ; c rho désigne le coefficient de corrélation des erreurs sur les ratios $^{238}U/^{206}Pb$ et $^{207}Pb/^{206}Pb$; d une analyse est qualifiée de concordante (« c ») si l'ellipse d'erreur intercepte la Concordia et discordante (« d ») si ce n'est pas le cas.

REFERENCES

Alexandre P. (2007) – U–Pb zircon SIMS ages from the French Massif Central and implication for the pre-Variscan tectonic evolution in Western Europe. C. R. Geosci., 339, 613–621.

Alexandrov P., Floc'h J.-P., Cuney M., Cheilletz A. (2001) – Ion microprobe dating of zircons from the Upper Gneiss Unit (South Limousin, Massif Central, France). C. R. Acad. Sci. Paris, 332, 625–632.

Alvaro J.J., Bauluz B., Clausen S., Devaere L., Gil Imaz A., Monceret É., Vizcaïno D. (2014) – Stratigraphic review of the Cambrian-Lower Ordovician volcanosedimentary complexes from the northern Montagne Noire, France. Stratigraphy, 11, 83–96.

Barras E. (1979) – Le dôme "orthogneissique" de Montredon-Labessonnié (Tarn) et son enveloppe métamorphique. Thèse de 3ème cycle, Univ. de Toulouse, France, 170 p.

Béziat P., Prouhet J.-P., Tollon F. (1980) – Le district de Montredon-Labessonnié (Tarn) : W, Sn, F. Publications du 26ème Congrès Géologique International, 44 p.

Black L.P., Kamo S.L., Allen C.M., Aleinikoff J.N., Davis D.W., Korsch R.J., Foudoulis C. (2003) – TEMORA 1: a new zircon standard for phanerozoic U–Pb geochronology. Chem. Geol., 200, 155–170.

Bonin B., Janoušek V., Moyen J.-F. (2020) – Chemical variation, modal composition and classification of granitoids. Geol. Soc. Lond. Spec. Publ., 491, 9–51.

Brown M., D'Lemos R.S. (1991) – The Cadomian granites of Mancellia, northeast Armorican Massif of France: relationship to the St. Malo migmatite belt, petrogenesis and tectonic setting. Precambrian Res., 51, 393–427.

Chantraine J., Autran A., Cavelier C. (1996) – Carte géologique de la France à l'échelle du millionième, 6ème édition. BRGM, Orléans.

Chelle-Michou C., Laurent O., Moyen J.-F., Block S., Paquette J.-L., Couzinié S., Gardien V., Vanderhaeghe O., Villaros A., Zeh A. (2017) – Pre-Cadomian to late-Variscan odyssey of the eastern Massif Central, France: Formation of the West European crust in a nutshell. Gondwana Res., 46, 170–190.

Cocherie A., Baudin T., Autran A., Guerrot C., Fanning C.M., Laumonier B. (2005) – U–Pb zircon (ID–TIMS and SHRIMP) evidence for the early Ordovician intrusion of metagranites in the late Proterozoic Canaveilles Group of the Pyrénées and the Montagne Noire (France). Bull. Soc. Geol. Fr., 176, 269–282.

Couzinié S. (2017) – Evolution of the continental crust and significance of the zircon record, a case study from the French Massif Central. Thèse de doctorat, Univ. de Lyon, France, 432 p.

Couzinié S., Laurent O., Poujol M., Mintrone M., Chelle-Michou C., Moyen J.-F., Bouilhol P., Vezinet A., Marko L. (2017) – Cadomian S-type granites as basement rocks of the Variscan belt (Massif Central, France): Implications for the crustal evolution of the north Gondwana margin. Lithos, 286–287, 16–34.

Couzinié S., Laurent O., Chelle-Michou C., Bouilhol P., Paquette J.-L., Gannoun A.-M., Moyen J.-F. (2019) – Detrital zircon U–Pb–Hf systematics of Ediacaran metasediments from the French Massif Central: Consequences for the crustal evolution of the north Gondwana margin. Precambrian Res., 324, 269–284.

Couzinié S., Bouilhol P., Laurent O., Marko L., Moyen J.-F. (2021) – When zircon drowns: Elusive geochronological record of water-fluxed orthogneiss melting in the Velay dome (Massif Central, France). Lithos, 384–385, 105938.

Corfu F., Hanchar J.M., Hoskin P.W.O., Kinny P.D. (2003) – Atlas of Zircon Textures. Rev. Mineral. Geochem., 53, 469–500

Debon F., Le Fort P. (1988) – A cationic classification of common plutonic rocks and their magmatic associations: principles, method, applications. Bull. Minéral., 111, 493–510.

Demange M. (1982) – Etude géologique du massif de l'Agout (Montagne Noire, France). Thèse d'Etat, Univ. Paris VI, France, 1055 p.

Demange M. (1994) – Antevariscan evolution of Montagne Noire (France): from a passive margin to a foreland basin. C. R. Acad. Sci. II, 318, 921–933.

Egal E., Guennoc P., Le Goff E., Thiéblemont D., Lebret P., Hallégouet B. (1996) – The Cadomian orogeny revisited in northern Brittany, in: Avalonian and Related Peri-Gondwanan Terranes of the Circum-North Atlantic. Geol. Soc. Am. Spec. Paper, 304, 281–318.

Faure M., Cocherie A., Be Mezeme E., Charles N., Rossi P. (2010) – Middle Carboniferous crustal melting in the Variscan Belt: New insights from U–Th–Pbtot monazite and U–Pb zircon ages of the Montagne Noire Axial Zone (southern French Massif Central). Gondwana Res., 18, 653–673.

Frost B.R., Barnes C.G., Collins W.J., Arculus R.J., Ellis D.J., Frost C.D. (2001) – A geochemical classification for granitic rocks. J. Petrol., 42, 2033–2048.

Garfunkel Z. (2015) – The relations between Gondwana and the adjacent peripheral Cadomian domain—constrains on the origin, history, and paleogeography of the peripheral domain. Gondwana Res. 28, 1257–1281.

Gèze B. (1949) – Etude géologique de la Montagne noire et des Cévennes méridionales. Mém. Soc. Géol. Fr., 62, 215 p.

Guérangé-Lozes J. (1987) – Les nappes varisques de l'Albigeois cristallin. Lithostratigraphie, volcanisme et déformations. Thèse d'Etat, BRGM, 459 p.

Guérangé-Lozes J., Burg J.-P. (1990) – Variscan nappes in the southwest of the Massif Central (1:250 000 geological and structural maps of Montpellier and Aurillac). Géol. Fr., 3–4, 71–106.

Guérangé-Lozes J., Demange M., Mouline M. (2013) – Notice explicative, Carte géol. France (1/50 000), feuille Castres (986). BRGM, Orléans, 195 p.

Guion J.-L. (1984) – Contribution à l'étude géologique et gitologique du district à tungstène, étain et fluor de Montredon- Labessonié (Tarn). Thèse de 3ème cycle, Univ. Toulouse 3, 172 p.

Hamet J., Allègre C.J. (1973) – Datation 87Rb–87Sr du massif granitique du Mendic et des prophyroïdes à l'est de la Montagne Noire – un exemple de relation entre pluton et volcans. Contrib. Mineral. Petrol., 38, 291–298.

Harlaux M., Romer R.L., Mercadier J., Morlot C., Marignac C., Cuney M. (2018) – 40 Ma of hydrothermal W mineralization during the Variscan orogenic evolution of the French Massif Central revealed by U–Pb dating of wolframite. Miner. Deposita, 53, 21–51.

Horstwood M.S.A., Košler J., Gehrels G., Jackson S.E., McLean N.M., Paton C., Pearson N.J., Sircombe K., Sylvester P., Vermeesch P., Bowring J.F., Condon D.J., Schoene B. (2016) – Community-Derived Standards for LA-ICP-MS U–(Th–)Pb Geochronology – Uncertainty Propagation, Age Interpretation and Data Reporting. Geostand. Geoanalytical Res., 40, 311–332.

Jaffey A.H., Flynn K.F., Glendenin L.E., Bentley W.C., Essling A.M. (1971) – Precision measurement of half-lives and specific activities of 235U and 238U. Phys. Rev., 4, 1889–1906.

Lafon J.M. (1984) – La granodiorite de Caplongue, nouveau témoin d'un magmatisme cambrien dans le Rouergue oriental. C. R. Acad. Sci. Paris, 298, 595–600.

Laumonier B., Autran A., Barbey P., Cheilletz A., Baudin T., Cocherie A., Guerrot C. (2004) – On the non-existence of a Cadomian basement in southern France (Pyrénées, Montagne Noire): implications for the significance of the pre-Variscan (pre-Upper Ordovician) series. Bull. Soc. Geol. Fr., 175, 643–655.

Lescuyer J.-L., Cocherie A. (1992) – Single-zircon dating of the Sériès meta-dacites: evidence for a Late Proterozoic age of the "X Schists" from Montagne Noire (Southern French Massif Central). C. R. Acad. Sci., II, 314, 1071–1077.

Linnemann U., Gerdes A., Hofmann M., Marko L. (2014) – The Cadomian Orogen: Neoproterozoic to Early Cambrian crustal growth and orogenic zoning along the periphery of the West African Craton—Constraints from U–Pb zircon ages and Hf isotopes (Schwarzburg Antiform, Germany). Precambrian Res., 244, 236–278

Lotout C., Pitra P., Poujol M., Van Den Driessche J. (2017) – Ordovician magmatism in the Lévézou massif (French Massif Central): tectonic and geodynamic implications. Int. J. Earth Sci., 106, 501–515.

Marini F. (1987) – Relictual clinopyroxenes in Paleozoic metabasites from Albigeois: tracers of a distensive transitional-to-tholeiitic volcanism ("Schistes et Roches Vertes" formation, Tarn, probable Ordovician age). C. R. Acad. Sci. II, 304, 29–34.

Melleton J., Cocherie A., Faure M., Rossi P. (2010) – Precambrian protoliths and Early Paleozoic magmatism in the French Massif Central: U–Pb data and the North Gondwana connection in the west European Variscan belt. Gondwana Res., 17, 13–25.

Padel M., Álvaro J.J., Clausen S., Guillot F., Poujol M., Chichorro M., Monceret É., Pereira M.F., Vizcaïno D. (2017) – U–Pb laser ablation ICP–MS zircon dating across the Ediacaran–Cambrian transition of the Montagne Noire, southern France. C. R. Geosci., 349(8), 380-390.

Padel M., Álvaro J.J., Casas J.M., Clausen S., Poujol M., Sánchez-García T. (2018) – Cadomian volcanosedimentary complexes across the Ediacaran–Cambrian transition of the Eastern Pyrenees, southwestern Europe. Int. J. Earth Sci., 107, 1579–1601.

Pin C., Lancelot J. (1978) – Un exemple de magmatisme cambrien dans le Massif Central : les métadiorites quartziques intrusives dans la série du Lot. Bull. Soc. Geol. Fr., 7, 203–208.

Pin C., Marini F. (1993) – Early Ordovician continental break-up in Variscan Europe: Nd-Sr isotope and trace element evidence from bimodal igneous associations of the Southern Massif Central, France. Lithos, 29, 177–196.

Pitra P., Poujol M., Van Den Driessche J., Poilvet J.-C., Paquette J.-L. (2012) – Early Permian extensional shearing of an Ordovician granite: The Saint-Eutrope "C/S-like" orthogneiss (Montagne Noire, French Massif Central). C. R. Geosci., 344, 377–384.

Pupin, J.P. (1980) – Zircon and granite petrology. Contrib. Mineral. Petrol., 73, 207–220.

Roger F., Respaut J.-P., Brunel M., Matte P., Paquette J.-L. (2004) – Première datation U–Pb des orthogneiss œillés de la zone axiale de la Montagne noire (Sud du Massif central) : nouveaux témoins du magmatisme ordovicien dans la chaîne Varisque. C. R. Geosci., 336, 19–28.

Seifert W., Rhede D., Thomas R., Förster H.-J., Lucassen F., Dulski P., Wirth R. (2011) –Distinctive properties of rock-forming blue quartz: inferences from a multi-analytical study of submicron mineral inclusions. Mineral. Mag., 75, 2519–2534.

Sláma J., Košler J., Condon D.J., Crowley J.L., Gerdes A., Hanchar J.M., Horstwood M.S.A., Morris G.A., Nasdala L., Norberg N., Schaltegger U., Schoene B., Tubrett M.N., Whitehouse M.J. (2008) – Plešovice zircon – A new natural reference material for U–Pb and Hf isotopic microanalysis. Chem. Geol., 249, 1–35.

Spencer C.J., Kirkland C.L., Taylor R.J.M. (2016) – Strategies towards statistically robust interpretations of in situ U–Pb zircon geochronology. Geosci. Front., 7, 581–589.

Vavra G. (1994) – Systematics of internal zircon morphology in major Variscan granitoid types. Contrib. Mineral. Petrol., 117, 331–344.

Vermeesch P. (2018) – IsoplotR: A free and open toolbox for geochronology. Geosci. Front., 9, 1479–1493.

Villaseca C., Barbero L., Herreros V. (1998) – A re-examination of the typology of peraluminous granite types in intracontinental orogenic belts. Trans. R. Soc. Edinburgh, 89, 113–119.

Wiedenbeck M., Allé P., Corfu F., Griffin W.L., Meier M., Oberli F., Von Quadt A., Roddick J.C., Spiegel W. (1995) – Three natural zircon standards for U–Th–Pb, Lu–Hf, trace element and REE analyses. Geostand. Newsl., 19, 1–23.